Trajectory-Assisted Electric Vehicle Billing for Electrified Roadways

Anjali Mandokhot, Vassilis Kekatos, Ashutossh Gupta, Dionysios Aliprantis, and Steve Pekarek
Elmore Family School of Electrical and Computer Engineering, *Purdue University*, West Lafayette, IN, USA
{amandokh,kekatos,gupta799,dionysios,spekarek}@purdue.edu

***Abstract*—Electrified roadways (ERs) equipped with dynamic wireless power transfer (DWPT) can charge electric vehicles (EVs) while in transit. Although the ER operator can accurately measure the energy delivered by each transmitter (Tx) coil, it cannot directly determine how much energy was consumed by each EV. This work addresses this challenge by casting EV billing as the problem of assigning roadway-side Tx energization sequences to GPS-estimated EV trajectories. The key idea is to align Tx energy measurements collected by the ER infrastructure with EV positioning data. Continuous-time EV trajectories are reconstructed from low-rate and noisy GPS measurements using Gaussian-process (GP) regression, while Tx energization sequences are associated with EVs using either a greedy algorithm or a mixed-integer linear program (MILP) that enforces physically meaningful assignment constraints. Once the assignment has been established, the energy consumed by each EV follows directly from the measured Tx energies. Numerical tests on a realistic INDOT-inspired synthetic testbed demonstrate that the proposed MILP eliminates incorrect EV billing under varying traffic conditions while leaving less than 0.04% of the delivered energy unbilled. The proposed GP model also naturally incorporates Doppler speed measurements, further improving trajectory estimation under realistic GPS positioning errors.**

***Index Terms*—In-motion charging, EV billing, Gaussian processes, mixed-integer linear programming.**

I. Introduction

ERs enabled with DWPT have been proposed to power EVs while in transit [1]. By extending driving range and reducing on-board battery capacity requirements, DWPT has the potential to accelerate EV adoption. An ER consists of transmitter (Tx) coils embedded beneath the pavement. As an EV equipped with a receiver (Rx) coil traverses the ER, it draws power proportional to the instantaneous Rx/Tx overlap [2]. All Tx coils within an ER segment are supplied by a common substation [3], allowing the ER operator to measure the energy delivered by each Tx coil throughout ER operation. These measurements, however, do not reveal how much of that energy was consumed by any individual EV. Accurately attributing metered Tx energy to individual vehicles is therefore a prerequisite for reliable EV billing, and is the problem addressed in this work.

While prior work has studied the impact of DWPT systems on the power grid [4], [5], proposed algorithms for sizing the supporting grid infrastructure [6], and developed control strategies for EV charging [7], the EV billing problem has received comparatively little attention. Existing approaches rely primarily on either onboard Rx power metering [8] or dedicated communication links that convey vehicle identity to the ER operator [9], [10]. These approaches, however, require additional sensing and communication infrastructure or fail to account for the time-varying nature of DWPT charging.

Unlike stationary EV charging, where the energy delivered to a vehicle is measured directly by a single charger [11], a DWPT-enabled EV receives energy sequentially from multiple Tx coils as it traverses the ER. Consequently, the ER operator observes only the energy delivered by individual Tx coils rather than the energy consumed by each vehicle. The principal challenge is therefore not measuring the roadway energy, but correctly associating each Tx energy data with the EV that generated it. Solving this data-association problem using only data already collected by the ER operator would eliminate the need for dedicated billing infrastructure and provide an independent mechanism for validating onboard metering. The proposed problem bears some resemblance to non-intrusive load monitoring (NILM), which seeks to recover individual loads from aggregate energy measurements [12]. Most NILM techniques, however, distinguish loads using characteristic temporal or spectral signatures [13]. Such approaches are not directly applicable to DWPT systems because EVs traveling at similar speeds can generate charging profiles with nearly identical frequency content [3].

In this context, the contributions of this work are to: *c1)* Solve the EV billing problem in an ER without onboard energy metering. The key idea is to match EV trajectories learned from GPS data to energy measurements collected directly on the ER infrastructure; *c2)* Develop a greedy and an MILP-based method to associate sequences of energized Tx coils with individual EVs. Although the MILP is computationally more demanding, it better handles assignment uncertainty and reduces incorrect EV billing; and *c3)* Propose a GP model to estimate EV trajectories from low-rate noisy GPS data. The proposed model naturally incorporates both positioning and Doppler speed measurements, thereby reducing uncertainty in EV trajectory estimation. Numerical tests on a realistic synthetic testbed show that the proposed methods accurately estimate EV energy consumption across a wide range of traffic conditions and GPS measurement noise levels.

II. System Modeling and Problem Statement

Let us briefly summarize a system model of the DWPT-enabled electrified roadway (ER). We study an ER segment

This work was supported in part by US NSF grants 2500682 and 1941524.

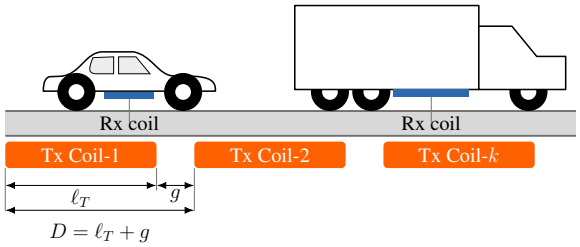

Fig. 1. Cross-section of the DWPT lane.

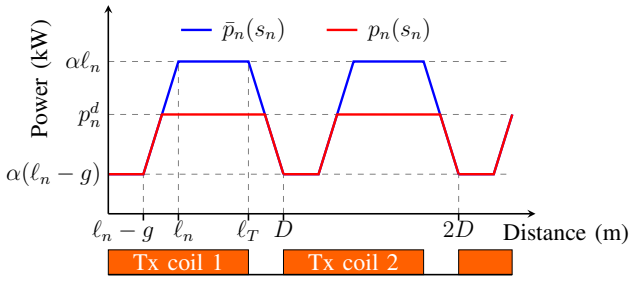

Fig. 2. The blue curve shows the maximum power an EV can consume when positioned at distance s_n. The available power is maximized when the entire length of the Rx coil is positioned above a Tx coil, and the Rx coil is positioned above a Tx coil slab gap. The red curve shows a possible actual EV load profile where the EV energy management system truncates the consumed power to the needed peak demand p_n^d.

of length L in meters, served by a single power substation. Without loss of generality, we consider traffic flow in a single direction and assume that the DWPT technology has been deployed on the rightmost ER lane [14]. The ER powers EVs via electromagnetic induction using a series of transmitter (Tx) coils installed periodically beneath the pavement. Each Tx coil is of length ℓ_T meters and is followed by a g-meter-long gap, as shown in Fig. 1. A Tx coil and the subsequent gap form a *coil segment* of length

$$D = \ell_T + g. \tag{1}$$

The ER segment has $K = L/D$ segments indexed by k.

Consider the problem of billing EVs powered by this ER segment over the interval $\mathcal{T} := [0, T]$. During this interval, the ER segment powers a set $\mathcal{N}$ EVs, indexed by $n = 1, \ldots, N$. Given EV positioning data and Tx coil energy measurements, our goal is to estimate the total energy consumed by each EV as it traverses the ER segment during $\mathcal{T}$. This billing task becomes straightforward if each EV is equipped with an onboard energy meter. Instead, we develop a billing solution that does not require onboard energy measurements for two reasons. *r1)* Implementing revenue-grade sensing hardware at DWPT-level electrical ratings, while meeting the rugged packaging requirements for equipment mounted beneath heavy-duty vehicles, would increase both system complexity and cost. *r2)* Even if EVs are equipped with meters, an independent billing mechanism remains valuable for cross-validation and resilience against meter failures or cyber-attacks.

To describe the data available for EV billing, we first present a model of EV charging profiles. Each EV is equipped with a receiver (Rx) coil of length ℓ_n, measured in meters. Without loss of generality, we assume $\ell_n < \ell_T$ for all n. For now, suppose that EV$_n$ travels exactly along the centerline of the DWPT lane. Let s_n denote its distance from the beginning of the ER segment measured along the lane. The blue curve in Fig. 2 depicts the maximum charging power $\bar{p}_n(s_n)$ available to EV$_n$ at position s_n. This maximum power depends on the Rx/Tx coil overlap and the ER system's power density α, expressed in kW/m of Rx/Tx overlap [3]. Consequently, the maximum power $\bar{p}_n(s_n)$ is a periodic trapezoidal function with period D. An EV$_n$ may consume less than $\bar{p}_n(s_n)$. In current DWPT implementations, the EV energy management system specifies a desired charging power p_n^d, while the power converter limits the actual charging power $p_n(s_n)$ at position s_n according to the clipping control law [2], [15]:

$$p_n(s_n) = \begin{cases} p_n^d, & p_n^d \le \bar{p}_n(s_n) \\ \bar{p}_n(s_n), & \text{otherwise.} \end{cases} \tag{2}$$

The red curve in Fig. 2 shows this control law for some p_n^d.

Given the vehicle speed, the EV load profile $p_n(s_n)$ can be expressed as a function of time. Specifically, if EV$_n$ travels at a constant speed v_n, its time-domain load profile $p_n(t)$ retains the same periodic trapezoidal shape, with period D/v_n. More generally, if the vehicle speed varies over time, $p_n(t)$ still consists of a sequence of trapezoidal pulses whose durations vary according to the speed profile. The EV billing task is to compute the energy delivered to each EV:

$$E_n = \int_0^T p_n(t)\mathrm{d}t. \tag{3}$$

Unfortunately, the ER operator cannot directly measure $p_n(t)$ or E_n. Moreover, the stylized model of $p_n(t)$ described earlier becomes more complex in practice for three reasons. First, depending on propulsion, battery charging, and auxiliary loads, the desired charging power p_n^d may vary over time. Second, lateral misalignment relative to the DWPT lane centerline reduces Rx/Tx overlap and, consequently, the maximum available charging power. Third, during overtaking maneuvers, an EV may temporarily leave the DWPT lane.

Rather than relying on onboard energy measurements, our billing method uses two data sources. *ER data.* Whenever a Tx coil transfers energy to an EV, the ER operator records the Tx coil index, the timestamp of the transfer, and the delivered energy in Wh. The Tx coil index can be directly mapped to distance because the operator knows that coil k is located at distance kD from the beginning of the ER segment. *Vehicle data.* For each EV, the ER operator collects timestamped GPS measurements, including the EV position in Cartesian coordinates (in meters) and its speed in the direction of travel (in m/s). Unlike the Tx measurements, GPS data collected from moving vehicles are typically sparse and noisy [16]. For example, with a GPS sampling rate of 1 Hz, an EV traveling at 24.6 m/s (55 mph) passes over approximately 5.4 Tx coil slabs between consecutive GPS measurements. Moreover, GPS observations typically exhibit a standard deviation of 1–5 m in position and 0.1 m/s in speed [16], [17]. We assume that

each EV is authenticated upon entering the ER segment, so that the operator knows the exact arrival time of each EV.

Before closing this section, we summarize the technical characteristics of a pilot ER project for reference.

Remark 1 (INDOT ER testbed)**.** *The INDOT and Purdue University ER testbed is a quarter-mile testbed on US-52/231 in West Lafayette, Indiana, designed to wirelessly charge heavy-duty electric trucks at highway speeds. It is the first U.S. highway project to successfully transfer high-power levels (up to 200 kW) to Class 8 trucks in motion, with operating voltages up to 800 V and output currents up to 360 A; see [15]. Its specifications are* $\ell_T = 3.66$ *m,* $g = 0.91$ *m,* $D = 4.57$ *m, and* $\alpha = 109.36$ *kW/m. The speed limit is* $v = 24.6$ *m/s or 55 mph. The pilot includes a prototype DWPT-enabled Class-8 truck with* $\ell_n = 1.83$ *m.*

III. Proposed EV Billing Approach

The proposed EV billing approach includes three steps:

S1) Build energization sequences from Tx coil data;
S2) Estimate EV trajectories from GPS data; and
S3) Assign energization sequences to EVs.

In this section, we focus on *S1)* and *S3)*. The discussion on *S2)* is deferred to Sec. IV.

A. Step S1) Identify Tx Energization Sequences

The operator first processes the Tx coil measurements to construct *Tx energization sequences*. For example, if Tx coils $\{k, k+1, \ldots, k+100\}$ are energized in rapid succession, their timestamped energy measurements are grouped into a single energization sequence. Since these coils are energized consecutively over a short time interval, it is reasonable to attribute them to the passage of a single EV. Energization sequences are indexed by $i \in \{1, \ldots, I\}$. Each sequence i is characterized by:

- starting and ending times $[t_i^1, t_i^2] \subseteq \mathcal{T}$;
- position $z_i(t)$ along the DWPT lane for $t \in [t_i^1, t_i^2]$; and
- average charging power $p_i(t)$ for $t \in [t_i^1, t_i^2]$.

In the preceding example, the sequence begins at position $z_i(t_i^1) = kD$ and ends at position $z_i(t_i^2) = (k+100)D$. The power signal $p_i(t)$ is reconstructed from the energy measurements of the energized Tx coils within the sequence. Because Tx coil measurements are acquired at sufficiently high temporal resolution, both $z_i(t)$ and $p_i(t)$ can be reconstructed by interpolating the underlying discrete measurements.

To summarize, the first step of the proposed workflow stitches together consecutive Tx coil measurements to form Tx energization sequences. The remaining two steps assign these sequences to individual EVs. In the ideal case where EV_n remains on the DWPT lane throughout its traversal of the ER segment, it generates a single energization sequence i of relatively long duration, $t_i^2 - t_i^1$. This sequence can be reliably associated with EV_n based on its arrival time at the ER segment. The total energy delivered to EV_n is

$$E_n = \int_{t_i^1}^{t_i^2} p_i(t)\,\mathrm{d}t. \tag{4}$$

The integral can be computed from discrete-time samples of average power collected from Tx coil slabs.

In practice, however, an EV may repeatedly enter and leave the DWPT lane, producing multiple short energization sequences. The central challenge is to determine which sequences originate from the same EV. This cannot be accomplished reliably using Tx coil data alone, since multiple EVs may generate interleaved energization sequences while overtaking one another. Our key idea is to exploit vehicle trajectories to resolve this ambiguity. Specifically, we can assign multiple energization sequences to a single EV by matching the position signal of each sequence to the trajectory of a single EV. Once sequences have been assigned to EVs, the total electrical energy delivered to EV_n can be found as

$$E_n = \sum_{i \in \mathcal{I}_n} \int_{t_i^1}^{t_i^2} p_i(t)\,\mathrm{d}t, \tag{5}$$

where $\mathcal{I}_n$ is the subset of Tx sequences assigned to EV_n. The process of estimating EV trajectories from GPS data is postponed to Sec. IV. Before that, Section III-B explains how to assign sequences to vehicles.

B. Step S3) Assign Tx Energization Sequences to EVs

In this section, we assign Tx energization sequences to EVs by matching their trajectories on the ER's two-dimensional terrain. Instead of Cartesian coordinates (x, y), we elect to use the *Frenet coordinates* (s, d), defined by the DWPT lane centerline as follows: The *station* s is the distance along the DWPT lane from the beginning of the ER segment to the point (x, y). The *lateral offset* d is the signed perpendicular distance of the point from the centerline. Positive values of d correspond to positions on the left-hand side of the centerline in the direction of travel. Working with Frenet coordinates simplifies the tasks of learning and matching trajectories.

As discussed in Sec. III-A, the ER operator knows the trajectory of each sequence i in Frenet coordinates:

$$(z_i(t), 0) \quad \text{for} \quad t \in \left[t_i^1, t_i^2\right].$$

The lateral offset remains at zero because Tx coil slabs are located along the reference path. Regarding EV trajectories, suppose that the ER operator has estimated the trajectory of EV_n in Frenet coordinates:

$$(s_n(t), d_n(t)) \quad \text{for} \quad t \in \mathcal{T}.$$

The task of estimating the EV trajectories from GPS data is deferred to Section IV. Vehicles may have nonzero offsets if they switch lanes. To assign sequences to EVs, we compute the time-averaged trajectory error across all sequence-EV pairs

$$D_{in} := \frac{1}{t_i^2 - t_i^1} \int_{t_i^1}^{t_i^2} \left(\left(z_i(t) - s_n(t)\right)^2 + d_n^2(t) \right) \mathrm{d}t. \tag{6}$$

Under exact trajectory information, sequence i can be assigned to the EV attaining the smallest trajectory error

$$n_i := \arg\min_{n \in \mathcal{N}} D_{in}. \tag{7}$$

Since each sequence is assigned independently of all others, we refer to this procedure as the *greedy approach*.

Despite its computational simplicity, this greedy approach may produce incorrect assignments when trajectory information is noisy. By construction, the minimization in (7) assigns each sequence to exactly one EV, which is a desirable property. Moreover, a single EV may be assigned multiple sequences. This is also a reasonable property because an EV can generate multiple sequences by repeatedly entering and leaving the DWPT lane. However, any two sequences assigned to the same EV must be non-overlapping in time. This is simply because an EV cannot be at two positions at the same time.

Noisy trajectory estimates may cause the greedy approach to assign temporally overlapping energization sequences to the same EV, particularly for short sequences. Moreover, when the minimum trajectory error in (7) exceeds a threshold $D_{\min}$, assigning sequence i to EV_{n_i} may result in incorrect billing. To avoid overcharging EVs, such sequences are left *unassigned*. The threshold $D_{\min}$ can be chosen as four times the median trajectory error computed from historical or simulated data.

To address these two challenges, we propose assigning sequences to EVs in a coordinated rather than independent manner. First, identify all pairs of temporally overlapping sequences and place them in the set

$$\mathcal{O} := \left\{(i,j) : [t_i^1, t_i^2] \cap [t_j^1, t_j^2] \neq \varnothing\right\}. \tag{8}$$

Given $\mathcal{O}$, we assign sequences to EVs using the MILP:

$$\min \quad \sum_{i\in\mathcal{I}} \sum_{n\in\mathcal{N}} b_{in}\left(D_{in} - D_{\min}\right) \tag{9a}$$

$$\text{over} \quad b_{in} \in \{0,1\}, \quad \forall i \in \mathcal{I}, n \in \mathcal{N} \tag{9b}$$

$$\text{s.to} \quad \sum_{n\in\mathcal{N}} b_{in} \leq 1, \quad \forall i \in \mathcal{I} \tag{9c}$$

$$b_{in} + b_{jn} \leq 1, \quad \forall (i,j) \in \mathcal{O}, n \in \mathcal{N}. \tag{9d}$$

Variable b_{in} takes the value of 1 if sequence i is assigned to EV_n; and zero, otherwise. Constraint (9d) prevents any two overlapping sequences from being assigned to the same EV. Constraint (9c) ensures that each sequence is assigned to at most one EV. If for sequence i, it holds

$$\min_{n\in\mathcal{N}} D_{in} \geq D_{\min},$$

all cost coefficients become positive and the MILP decides $b_{in} = 0$ for all n, i.e., the sequence remains unassigned. Otherwise, at least one of the cost coefficients $(D_{in} - D_{\min})$ is negative. In this case, the MILP sets $b_{in} = 1$ for the EV_n with the most negative cost coefficient.

IV. Estimating EV Trajectories from GPS Data

Switching to Step *S2)*, this section explains how the ER operator can estimate EV trajectories in Frenet coordinates from low-rate noisy GPS data. We first map the GPS measurements from Cartesian to Frenet coordinates (Sec. IV-A), then estimate the EV trajectories using GP regression (Sec. IV-B), and finally show how speed measurements can be incorporated to improve trajectory estimation (Sec. IV-C).

A. Projection onto Frenet Coordinates

Let us parameterize the DWPT lane centerline in Cartesian coordinates by the station $s \in [0, L]$ as

$$\mathbf{r}(s) = \begin{bmatrix} x(s) & y(s) \end{bmatrix}^\top. \tag{10}$$

Let $\mathbf{p} = [x\ y]^\top$ denote an EV position reported by the GPS receiver in Cartesian coordinates. The Frenet coordinates (s, d) of this $\mathbf{p}$ can be computed by projecting $\mathbf{p}$ onto $\mathbf{r}(s)$ [18]:

$$s = \arg\min_{\xi\in[0,L]} \|\mathbf{p} - \mathbf{r}(\xi)\|_2 \tag{11a}$$

$$d = (\mathbf{p} - \mathbf{r}(s))^\top \mathbf{n}(s), \tag{11b}$$

where $\mathbf{n}(s)$ is the unit normal vector to the DWPT lane centerline at position s.

Applying this projection to every GPS sample yields noisy observations of the EV trajectory in Frenet coordinates

$$\hat{s}(t_m) = s(t_m) + w_s(t_m), \tag{12a}$$

$$\hat{d}(t_m) = d(t_m) + w_d(t_m), \tag{12b}$$

sampled at times $\{t_m\}_{m=1}^M$. The actual EV coordinates (s, d) are corrupted by measurement noise (w_s, w_d) to yield the observed EV coordinates $(\hat{s}, \hat{d})$. The GPS measurement noise can be modeled as zero-mean Gaussian. Standard deviations of 1–5 m are typical for vehicles in motion. Noise is independent across the two Cartesian coordinates. If the highway can be locally approximated by a straight line, the noise can be approximated as independent across Frenet coordinates as well. Because GPS data are noisy and low-rate, they cannot be directly matched with high-rate Tx energization data. To address this issue, we use GPS data to train a Gaussian process (GP) model for each EV trajectory. Once learned, we can sample this GP model at any time instance.

B. Gaussian-Process Trajectory Estimation

Let us first briefly review the basics of GPs. A GP is a random process such that any finite collection of its samples forms a Gaussian random vector. Consider a time series $s(t)$ and two sets of time indices $\mathcal{T}_1$ and $\mathcal{T}_2$. The time series $s(t)$ is a GP if the two vectors $\mathbf{s}_1$ and $\mathbf{s}_2$ collecting samples of $s(t)$ over $\mathcal{T}_1$ and $\mathcal{T}_2$ are jointly Gaussian or

$$\mathbf{s} = \begin{bmatrix} \mathbf{s}_1 \\ \mathbf{s}_2 \end{bmatrix} \sim \mathcal{N}\left(\begin{bmatrix} \boldsymbol{\mu}_1 \\ \boldsymbol{\mu}_2 \end{bmatrix}, \begin{bmatrix} \boldsymbol{\Sigma}_{11} & \boldsymbol{\Sigma}_{21}^\top \\ \boldsymbol{\Sigma}_{21} & \boldsymbol{\Sigma}_{22} \end{bmatrix}\right). \tag{13}$$

Based on (13), the conditional pdf of $\mathbf{s}_2$ given $\mathbf{s}_1$ is also Gaussian with mean

$$\mathbb{E}[\mathbf{s}_2|\mathbf{s}_1] = \boldsymbol{\mu}_2 + \boldsymbol{\Sigma}_{21}\boldsymbol{\Sigma}_{11}^{-1}(\mathbf{s}_1 - \boldsymbol{\mu}_1). \tag{14}$$

The GP model is useful because, upon observing $\mathbf{s}_1$, the value in (14) is the minimum mean-square error (MMSE) estimator of $\mathbf{s}_2$. For the model to be practical, we should be able to express the mean and covariances in (13) for any time indices.

For simplicity, we model the two Frenet coordinates using independent GPs. The longitudinal trajectory is modeled as

$$s(t) \sim \mathcal{GP}\left(\mu_s(t), k_s(t,t')\right). \tag{15}$$

The mean value function is modeled as

$$\mu_s(t) = v_0\,(t - t_0)\,u(t - t_0), \tag{16}$$

where v_0 and t_0 are the average speed and the arrival time for this EV, respectively, and $u(\tau)$ is the unit step function. The covariance function is modeled using the Gaussian kernel

$$k_s(t, t') = \alpha_s e^{-\beta_s (t-t')^2} + \sigma_w^2 \delta(t - t'), \tag{17}$$

where (α_s, β_s) are learned by maximizing the GP marginal likelihood using the available GPS data; σ_w^2 is the GPS noise variance; and $\delta(\tau)$ is the Kronecker delta function.

The vector $\mathbf{s}_1$ in (13) contains all M GPS longitudinal observations for EV$_n$ from (12a). To compute the trajectory mismatch D_{in} in (7), we must sample EV$_n$'s trajectory $(s_n(t), d_n(t))$ at the time instants corresponding to the samples of the energization sequence i during $[t_i^1, t_i^2]$. The vector $\mathbf{s}_2$ collects these higher-frequency samples of $s_n(t)$, and can be obtained via the MMSE estimator in (14).

Similarly, the GP model for the lateral coordinate is

$$d(t) \sim \mathcal{GP}\left(0, k_d(t, t')\right). \tag{18}$$

The mean function is set to zero because the EV is expected to remain on the DWPT lane most of the time. The covariance function is defined similarly to the longitudinal one as

$$k_d(t, t') = \alpha_d e^{-\beta_d (t-t')^2} + \sigma_w^2 \delta(t - t'). \tag{19}$$

Once we have estimated $(s_n(t), d_n(t))$ at the sampling times of the energization sequence i, we can plug them into (6) to compute the trajectory error D_{in} for all i.

C. Incorporating Doppler Speed Measurements

Modern GPS receivers report not only vehicle position but also Doppler-based speed magnitude estimates in the direction of travel. Doppler speed measurements are less sensitive to satellite geometry and multipath effects, often achieving sub-meter-per-second accuracy. Speed measurements $v(t)$ are related to the longitudinal coordinate $s(t)$ because $v(t) = \dot{s}(t)$. We next explain how to leverage speed measurements to improve the estimates of longitudinal coordinates.

A fundamental property of GPs is that differentiation preserves Gaussianity. Consequently, if $s(t)$ is modeled as the GP in (15), then both the derivative process $v(t)$ and the joint process $\{s(t), v(t)\}$ remain Gaussian. Specifically, the mean is $\mathbb{E}[v(t)] = v_0$ and the related covariance functions are obtained by differentiating the kernel as

$$\mathrm{Cov}(s(t), v(t')) = \frac{\partial k_s(t, t')}{\partial t'}, \tag{20a}$$

$$\mathrm{Cov}(v(t), v(t')) = \frac{\partial^2 k_s(t, t')}{\partial t\, \partial t'} + \sigma_v^2 \delta(t - t'), \tag{20b}$$

where σ_v^2 is the noise variance for GPS speed data. Next, the observed vector $\mathbf{s}_1$ is augmented to include speed data along with the longitudinal data. Standard GP regression then yields the posterior trajectory $s_n(t)$ conditioned on both data sources.

TABLE I
BILLING PERFORMANCE UNDER DIFFERENT TRAFFIC CONDITIONS

Traffic	Method	Seq. (#)	Energy (kWh)	Incorrectly Assigned (%)	Unassigned (%)	Unbilled Energy (%)
Light	Greedy	213	728	0.94	0.47	< 0.001
	MILP			0.00	4.23	0.007
Medium	Greedy	479	1367	2.51	0.63	< 0.001
	MILP			0.00	5.64	0.026
Heavy	Greedy	760	1950	2.89	0.92	< 0.001
	MILP			0.00	6.71	0.035

V. NUMERICAL TESTS

The proposed EV billing methodology was numerically evaluated on a realistic synthetic testbed, as discussed next.

Electrified Roadway. We simulated a curved three-lane ER with DWPT technology deployed on the rightmost lane. The coil layout and speed specifications coincided with those of Remark 1. We simulated an ER length of $L = 4,000$ m over an observation period of $T = 1,440$ s.

Traffic simulation. We generated vehicle trajectories using SUMO, an open-source microscopic traffic flow simulator [19]. We simulated vehicle compositions of 53% class-9 trucks with Rx length $\ell_n = 1.83$ m, and 47% sedans with $\ell_n = 1.70$ m. Successive vehicles maintained a minimum spacing of 2.5 m and 1 s. To account for a worst-case assignment ambiguity, we assumed all vehicles were DWPT-enabled. EV load profiles were generated per (2). Peak demands p_n^d were fixed throughout the observation interval and drawn uniformly from $[15, 22]$ kW for sedans, and $[150, 190]$ kW for trucks.

EV positioning. SUMO returns vehicle trajectories in Cartesian coordinates. We sampled these trajectories at 100 Hz to reliably generate energization sequences. To synthesize GPS data, we downsampled the EV trajectories to 1 Hz and corrupted them with zero-mean white Gaussian noise. The noise standard deviation was set to $\sigma_v = 0.1$ m/s for speed data, and was varied across tests for positioning data.

Performance metrics. The billing approaches were evaluated in terms of the probability of incorrect assignment of an energization sequence to an EV, the probability of no assignment, and the total energy that was left unbilled.

We first tested the proposed methods across different traffic conditions. We simulated light, medium, and heavy traffic conditions by setting the mean vehicle arrival rate in SUMO as 0.30, 0.63, and 1.10 vehicles per second, respectively. The GPS noise standard deviation was kept fixed at 2 m. Table I reports the total number of energization sequences, total energy consumed, assignment error probabilities, and unbilled energy. The greedy approach incorrectly assigned approximately 1–3% of the energization sequences. The MILP features no incorrect assignments, but leaves 4–6% of sequences unassigned. However, those unassigned sequences accounted for only a negligible percentage of the total energy. This is because hard-to-assign sequences are typically extremely short.

We tested the MILP across different levels of noise in GPS position data. More specifically, the GPS noise standard

TABLE II
MILP PERFORMANCE OVER INCREASING GPS NOISE STD DEV

σ_w (m)	Incorrectly Assigned (%)	Unassigned (%)	Unbilled Energy (%)
2	0.00	5.64	0.026
3	0.00	5.01	0.022
4	0.00	5.64	0.024
5	0.42	5.43	0.022
6	0.42	5.43	0.023
7	0.63	5.85	0.024

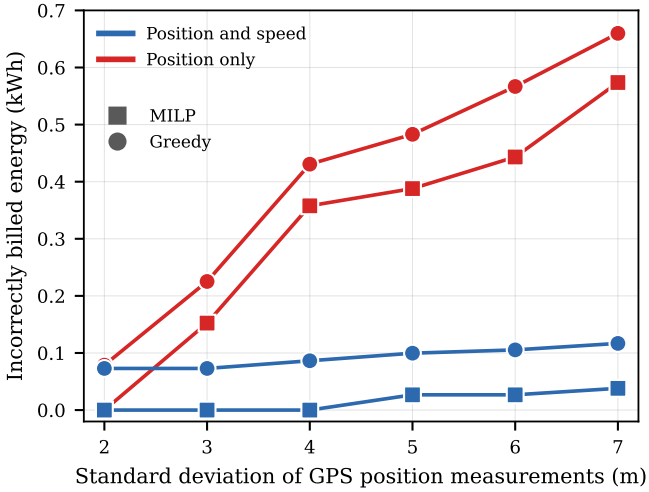

Fig. 3. Incorporating GPS speed measurements enhances EV trajectory estimation and yields more accurate sequence-to-EV assignments across varying GPS position-noise levels and medium traffic.

deviation was varied in $\sigma_w \in \{2, 3, \ldots, 7\}$ m. All tests were performed under the medium-traffic condition. As listed in Table II, there were no incorrect assignments up to the noise level of 4 m. Even at the noise level of 7 m, only 0.63% of assignments were incorrect. The unbilled energy never exceeded 0.03%. The previous tests leveraged both position and speed data. Figure 3 shows the total incorrectly billed energy, with and without accounting for speed, under medium-traffic conditions and over different noise levels for GPS position data. The performance of both methods improves with the addition of speed measurements, as expected. It is also clear that the MILP outperforms the greedy method in terms of energy incorrectly billed.

VI. CONCLUSIONS

We have formulated EV billing in DWPT-enabled ERs as the problem of assigning Tx energization sequences to EV trajectories estimated from GPS data. Numerical tests on a realistic synthetic testbed showed that the proposed MILP-based assignment eliminates incorrect EV billing over a wide range of traffic conditions by conservatively leaving only a small fraction of ambiguous sequences unassigned. Importantly, although approximately 4–6% of the sequences remain unassigned, they account for less than 0.04% of the total delivered energy because they are typically short-duration. The results also demonstrate that the proposed GP framework remains robust under realistic GPS positioning errors, while naturally incorporating Doppler speed measurements to further improve billing accuracy. Future work will investigate probabilistic sequence assignment using the full GP posterior and experimental validation on the INDOT DWPT testbed.

REFERENCES

[1] D. Haddad, T. Konstantinou, A. Prasad, Z. Hua, D. Aliprantis, K. Gkritza, and S. Pekarek, "Data-driven design and assessment of dynamic wireless charging systems," in *IEEE PELS Workshop on Wireless Power Transfer*, London, UK, Jun. 2019, pp. 59–64.

[2] A. Gupta, V. Kekatos, D. Aliprantis, and S. Pekarek, "Dynamic modeling of load demand in electrified highways based on the EV composition," in *Proc. IEEE PES General Meeting*, Montreal, Canada, Jul. 2026.

[3] A. Gupta, V. Kekatos, R. Yang, D. Aliprantis, and S. Pekarek, "Frequency-domain characterization of load demand from electrified highways," *IEEE Trans. Power Syst.*, 2026.

[4] A. Sauter, J. D. Lara, J. Turk, J. Milford, and B.-M. Hodge, "Power system operational impacts of electric vehicle dynamic wireless charging," *Applied Energy*, vol. 364, p. 123002, Jun. 2024.

[5] T. M. Newbolt, P. Mandal, H. Wang, and R. Zane, "Diverse effects of dynamic wireless power transfer roadway in-motion electric vehicle charging," in *Proc. IEEE Conf. on Innovative Smart Grid Technologies*, Washington, DC, Jan. 2023, pp. 1–5.

[6] D. Ghose, J. Qin, and S. Sivaranjani, "Traffic-aware microgrid planning for dynamic wireless electric vehicle charging roadways," 2026. [Online]. Available: https://arxiv.org/abs/2511.00941

[7] Y. Dong, J. Qin, S. Sivaranjani, X. Lu, D. Aliprantis, and D. Love, "Real-time charging control for electric roadways: Formulation and causal algorithms," in *Proc. IEEE PES General Meeting*, Seattle, WA, Jul. 2024.

[8] D. Zou, J. Liu, Y. Chen, Y. Liu, and Z. Chu, "Research on electric energy metering and charging system for dynamic wireless charging of electric vehicle," in *Proc. 4th Int. Conf. Intell. Transp. Eng.*, Singapore, Sep. 2019, pp. 252–255.

[9] T. Bianchi, A. Brighente, and M. Conti, "DynamiQS: Quantum secure authentication for dynamic charging of electric vehicles," in *Proc. of the ACM Conf. on Secur. and Priv. in Wirel. and Mob. Netw.*, Seoul, South Korea, May 2024, pp. 174–184.

[10] S. Asokraj, T. Bianchi, A. Brighente, M. Conti, and R. Poovendran, "Identity-based authentication for on-demand charging of electric vehicles," *IEEE Trans. on Dependable and Secur. Comput.*, vol. 22, no. 3, pp. 2492–2504, May 2024.

[11] S. S. Acharige, M. E. Haque, M. T. Arif, N. Hosseinzadeh, K. N. Hasan, and A. M. T. Oo, "Review of electric vehicle charging technologies, standards, architectures, and converter configurations," *IEEE Access*, vol. 11, pp. 41 218–41 255, 2023.

[12] P. A. Schirmer and I. Mporas, "Non-intrusive load monitoring: A review," *IEEE Trans. Smart Grid*, vol. 14, no. 1, pp. 769–784, Jan. 2023.

[13] X. Wu, X. Han, L. Liu, and B. Qi, "A load identification algorithm of frequency domain filtering under current underdetermined separation," *IEEE Access*, vol. 6, pp. 37 094–37 107, 2018.

[14] S. Bafandkar and A. Talebpour, "Charging while driving lanes: A boon to electric vehicle owners or a disruption to traffic flow," *Transportation Research Part A: Policy and Practice*, vol. 204, no. 104821, Feb. 2026.

[15] V. Mehar, N. Frooninckx, I. Abram, S. Pekarek, D. Aliprantis, A. Brovont, and R. Swanson, "Receiver-side power control of a 200-kW three-phase DWPT system for heavy-duty vehicles," in *Proc. Wireless Power Tech. Conf. and Expo*, Rome, Italy, Jun. 2025, pp. 172–177.

[16] Y. Du, J. Wang, C. Rizos, and A. El-Mowafy, "Vulnerabilities and integrity of precise point positioning for intelligent transport systems: Overview and analysis," *Satell. Navig.*, vol. 2, no. 1, p. 3, 2021.

[17] L. Ji, R. Sun, Q. Cheng, and J. Wang, "Evaluation of the performance of GNSS-based velocity estimation algorithms," *Satell. Navig.*, vol. 3, no. 1, p. 18, 2022.

[18] E. Héry, S. Masi, P. Xu, and P. Bonnifait, "Map-based curvilinear coordinates for autonomous vehicles," in *in Proc. Intl. Conf. Intell. Transp. Syst.*, Yokohama, Japan, Oct. 2017, pp. 1699–1705.

[19] P. A. Lopez, M. Behrisch, L. Bieker-Walz, J. Erdmann, Y.-P. Flötteröd, R. Hilbrich, L. Lücken, J. Rummel, P. Wagner, and E. Wießner, "Microscopic traffic simulation using SUMO," in *Proc. Intl. Conf. on Intell. Transp. Syst.*, Maui, HI, Nov. 2018, pp. 2575–2582.